Shear stabilization of miscible displacement processes in porous media

A. Rogerson
Center for Fluid Mechanics, Division of Applied Mathematics, Brown University, Providence, Rhode Island 02912

E. Meiburg
Department of Aerospace Engineering, University of Southern California, Los Angeles, California 90089-1191

(Received 5 October 1992; accepted 27 January 1993)

The interface region between two fluids of different densities and viscosities in a porous medium in which gravity is directed at various angles to the interface is analyzed. Under these conditions, base states exist that involve both tangential and normal velocity components. These base states support traveling waves. In the presence of a normal displacement velocity, the amplitude of these waves grows according to the viscous fingering instability. For the immiscible case, it can easily be shown that the growth rate is not affected by the tangential velocities, while surface tension results in the usual stabilization. For the case of two miscible fluids, the stability of the base states using the quasi-steady-state approximation is investigated. The resulting equations are solved analytically for time $t=0$ and a criterion for instability is formulated. The stability of the flow for times $t>0$ is investigated numerically using a spectral collocation method. It is found that the interaction of pressure forces and viscous forces is modified by tangential shear as compared to the classical problem, resulting in a stabilizing effect of the tangential shear. The key to understanding the physical mechanism behind this stabilization lies in the vorticity equation. While the classical problem gives rise to a dipole structure of the vorticity field, tangential shear leads to a quadrupole structure of the perturbation vorticity field, which is less unstable. This quadrupole structure is due to the finite thickness of the tangential base state velocity profile, i.e., the finite thickness of the dispersively spreading front, and hence cannot emerge on the sharp front maintained in immiscible displacements.

I. INTRODUCTION

Two-phase displacements in porous media or, by analogy, in Hele–Shaw cells, have long enjoyed the attention of researchers interested in applications such as enhanced oil recovery. More recently, attempts to gain an improved understanding of these flows have given rise to challenging theoretical and computational problems, which has led to their study from a more fundamental point of view. A comprehensive review of progress in the field is provided by Homsy.[1] For the basic stability problem of a plane interface displaced by flow normal to it, Saffman and Taylor,[2] as well as Chuoke *et al.*,[3] provided quantitative results concerning the growth rate and the stabilizing influence of surface tension. Tan and Homsy[4] performed the stability analysis for two miscible, neutrally buoyant fluids subject to a normal displacement velocity. The analysis of Yortsos and Zeybek[5] investigated the role of velocity-dependent dispersion on the stability of small-wavelength perturbations. More recently, Bacri *et al.*[6] conducted three-dimensional (3-D) experiments, comparing the data to their stability analysis, which included both gravity and nonlinear dispersion, as well as to other numerical investigations of viscous fingering. Also, Zeybek and Yortsos[7,8] discussed the parallel flow of two immiscible fluids in a Hele–Shaw cell. As they point out, parallel flow develops in thin oil reservoirs, in relative permeability measurements, and in countercurrent imbibition. Zeybek and Yortsos conducted experiments in which the plane of the Hele–Shaw apparatus is oriented perpendicularly to the direction of gravity. They observed traveling waves of apparently solitary nature along the interface, which was confirmed by weakly nonlinear asymptotic theory. Their investigation raises the question as to which flow configurations give rise to traveling wave solutions, and what the stability characteristics of such solutions are. The present study intends to answer this question by extending previous stability analyses and allowing for global velocities not only in the direction normal to the interface, but also parallel to it. In Sec. II we present the equations, base-state solution, and stability analysis in which both surface tension and diffusion are neglected. In Sec. III we demonstrate how these results are extended to include the effect of surface tension for two immiscible fluids. In Sec. IV we focus on two-phase miscible displacement, formulating the linear stability problem, solving it analytically at $t=0$, and establishing a criterion for instability. The solution to the stability problem is found numerically for $t>0$. In Sec. V we discuss the numerical method used to solve the stability problem for $t>0$, present the results obtained, and compare these results with those for the immiscible cases. Finally, we summarize our conclusions in Sec. VI.

II. TWO-PHASE DISPLACEMENT WITHOUT SURFACE TENSION OR DIFFUSION

We consider the two-dimensional configuration of a porous medium of constant permeability containing two fluids separated by a sharp interface (Fig. 1). The fluids

 0899-8213/93/061344-12$06.00

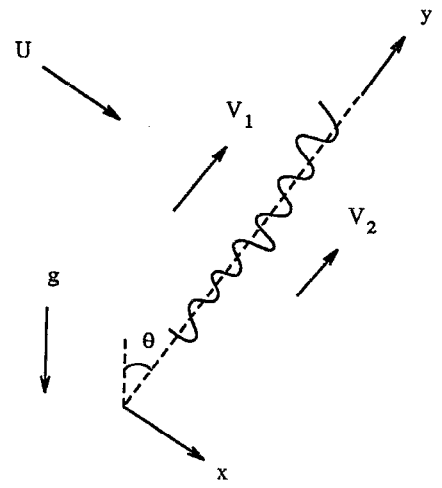

FIG. 1. Flow configuration. The interface is aligned along the y axis. Here U is a global displacement velocity normal to the interface in the x direction, while V_1 and V_2 are velocities tangential to the interface. The angle between the interface and gravity is denoted by θ.

move with velocities $\mathbf{u}_1$ and $\mathbf{u}_2$, respectively, in an incompressible fashion, so that the continuity equation reads as

$$\nabla \cdot \mathbf{u}_i = 0, \tag{1}$$

for $i=1,2$. Pressure, viscous, and gravitational forces obey Darcy's law,

$$\nabla p_i = -\mu_i \mathbf{u}_i + \rho_i \mathbf{g}, \tag{2}$$

where μ denotes the dynamic viscosity divided by the permeability. The fluid phases have respective densities ρ_1 and ρ_2, p denotes the pressure, and $\mathbf{g}$ is the gravitational acceleration. At the interface, the fluids' motion obeys the familiar conditions of equal normal velocities and pressures. Our goal then is to determine under which conditions the system described above allows for the the existence of base states involving straight interfaces, and to describe the stability characteristics of these base states.

A. Base state

We introduce a coordinate system whose y axis points along the interface, while the x axis has a direction normal to it (Fig. 1). Here U represents a global displacement velocity normal to the interface, while V_1 and V_2 denote the respective fluid velocity components tangential to the interface. If θ is the angle between the interface and the direction of gravity as depicted in Fig. 1, Darcy's law becomes

$$\mathbf{u}_i = -\frac{1}{\mu_i} \nabla [\, p_i + \rho_i g(-x \sin\theta + y \cos\theta)\,] = \nabla \phi_i, \tag{3}$$

where ϕ_i denotes the respective velocity potentials in the two fluid phases. The kinematic boundary condition of equal normal velocities at $x=0$ now yields

$$\left.\frac{\partial \phi_1}{\partial x}\right|_{x=0} = \left.\frac{\partial \phi_2}{\partial x}\right|_{x=0}, \tag{4}$$

while the equal pressure constraint at $x=0$ results in

$$\mu_1 \phi_1 + \rho_1 g y \cos\theta = \mu_2 \phi_2 + \rho_2 g y \cos\theta. \tag{5}$$

It is now straightforward to see that

$$\phi_1(x,y) = Ux + V_1 y, \tag{6}$$

$$\phi_2(x,y) = Ux + V_2 y, \tag{7}$$

satisfy the above equations and boundary conditions, provided that

$$V_2 = \frac{\mu_1}{\mu_2} V_1 - g \cos\theta \frac{\rho_2 - \rho_1}{\mu_2}. \tag{8}$$

Hence we recognize that for any combination of fluid densities and viscosities, and for arbitrary angles of inclination θ, there exists a V_2 for every V_1, such that the resulting flow represents an exact solution to the governing equations. Equation (8) merely states that the combination of V_1 and V_2 has to be such that along the interface, pressure gradients due to viscous forces exactly balance those due to gravity. Furthermore, we notice that V_1 and V_2 are not affected by U, so that a valid combination of V_1 and V_2 satisfies the governing equations, regardless of the overall displacement velocity U. We now proceed to investigate the stability characteristics of the above base state.

B. Stability analysis

If we introduce a small perturbation resulting in the interfacial position

$$x = x'(y), \tag{9}$$

the velocity potential can be written as

$$\phi_i = \phi_i^0 + \phi_i', \tag{10}$$

where the superscript, 0, refers to the base state derived above, and $'$ denotes the perturbation potential. The continuity equation (1) immediately yields

$$\nabla^2 \phi_i' = 0, \tag{11}$$

and the condition of decaying perturbations far away from the interface gives

$$\nabla \phi_1' \to 0, \quad \text{as } x \to -\infty, \tag{12}$$

$$\nabla \phi_2' \to 0, \quad \text{as } x \to +\infty. \tag{13}$$

We use the method of normal modes and assume

$$x'(y) = a e^{iky + \sigma t}, \tag{14}$$

$$\phi_1'(x,y) = \hat{\phi}_1(x) e^{iky + \sigma t}, \tag{15}$$

$$\phi_2'(x,y) = \hat{\phi}_2(x) e^{iky + \sigma t}. \tag{16}$$

The boundary conditions at infinity then require

$$\hat{\phi}_1(x) = A e^{kx}, \tag{17}$$

$$\hat{\phi}_2(x) = B e^{-kx}. \tag{18}$$

The linearized boundary conditions at the interface for the normal velocity,

$$\left.\frac{\partial \phi_i'}{\partial x}\right|_{x=0} = \frac{\partial x'}{\partial t} + V_i \frac{\partial x'}{\partial y}, \tag{19}$$

and the pressure,

$$-\mu_1[Ux' + \phi_1'(x=0,y)] + \rho_1 g x' \sin\theta$$
$$= -\mu_2[Ux' + \phi_2'(x=0,y)] + \rho_2 g x' \sin\theta, \tag{20}$$

then result in the growth rate,

$$\sigma = \frac{kU(\mu_2-\mu_1)}{\mu_1+\mu_2} + \frac{k(\rho_1-\rho_2)g\sin\theta}{\mu_1+\mu_2} - i\frac{k(V_1\mu_1+V_2\mu_2)}{\mu_1+\mu_2}. \tag{21}$$

Notice that the real part of the growth rate for $\theta=\pi/2$ corresponds to the result obtained for a horizontal interface subject to a normal displacement velocity U only, as stated by Saffman and Taylor.[2] However, we now have an additional, imaginary component of the growth rate, indicating the existence of traveling waves. Their phase velocity is a viscosity-weighted average of the tangential velocity components of the two fluids, so that the waves tend to travel with the more viscous phase. In particular, when $\mu_1=\mu_2$, the waves travel with the average velocity of the the two fluids, and when $V_1=V_2$, the waves travel with the same velocity as the fluids. Furthermore, we recognize that a vertical interface satisfying (8) without a normal displacement velocity is neutrally stable for all combinations of viscosities and densities, and allows for neutrally stable traveling waves.

III. IMMISCIBLE DISPLACEMENT: THE EFFECT OF SURFACE TENSION

If the interface between the two fluids gives rise to the surface tension γ, the boundary condition for the pressure (20) has to be modified. For small perturbations, the radius of curvature of the interface becomes inversely proportional to $\partial^2 x/\partial y^2$, and the accompanying pressure jump across the interface leads to

$$-\mu_1[Ux' + \phi_1'(x=0,y)] + \rho_1 g x' \sin\theta$$
$$= -\mu_2[Ux' + \phi_2'(x=0,y)] + \rho_2 g x' \sin\theta - \gamma\frac{d^2x}{dy^2}. \tag{22}$$

Consequently, the growth rate becomes

$$\sigma = \frac{kU(\mu_2-\mu_1)}{\mu_1+\mu_2} + \frac{k(\rho_1-\rho_2)g\sin\theta}{\mu_1+\mu_2} - \frac{\gamma k^3}{\mu_1+\mu_2} - i\frac{k(V_1\mu_1+V_2\mu_2)}{\mu_1+\mu_2}. \tag{23}$$

We find that surface tension stabilizes the traveling waves in the same way as for the classical nontraveling waves. The phase velocity of the waves remains unaffected.

A question of obvious interest concerns the evolution of the traveling waves if a normal displacement velocity causes their amplitudes to grow into the nonlinear regime. Along these lines, a numerical investigation employing Lagrangian boundary integral techniques[9] is currently underway. Brener *et al.*[10] have considered the selection of Saffman–Taylor fingers in the presence of gravity when the Hele–Shaw cell is rotated about the normal-flow direction, introducing constant tangential velocities.

IV. MISCIBLE DISPLACEMENT: THE EFFECT OF DIFFUSION

If the two phases are miscible; diffusion between the fluids represents an important physical mechanism in the evolution of instability waves. As Tan and Homsy[4] show in their stability analysis of rectilinear miscible displacements without the effect of gravity, it is diffusion that prevents the unbounded increase of the growth rate with the wave number by damping short waves. These authors employ a quasi-steady-state approximation (QSSA), i.e., they calculate the instability growth rates under the assumption that the time scale for the growth of instability waves is much shorter than the one governing the base flow. Their quantitative results are in good agreement with initial-value calculations and predict the spacing of experimentally observed viscous fingers reasonably well, thus lending support to the validity of the QSSA. Consequently, we will in the following employ the QSSA to investigate the stability of miscible displacement processes involving inclined interfaces. After presenting the governing equations and scaling them in the appropriate fashion, we will formulate the stability problem on the basis of the QSSA. Subsequently, we will solve the stability problem analytically at $t=0$. In Sec. V we discuss numerical results to the stability problem for $t>0$.

A. Governing equations and base state

We assume incompressible flow in a homogeneous medium of constant permeability, as sketched in Fig. 1. In a reference frame moving in the x direction with average displacement velocity U, the equations governing the motion of two fluids subject to a constant diffusion coefficient D are

$$\nabla\cdot\mathbf{u}=0, \tag{24}$$

$$\nabla p = -\mu(\mathbf{u}-U\mathbf{e}_x) + \rho\mathbf{g}, \tag{25}$$

$$\frac{\partial c}{\partial t} + \mathbf{u}\cdot\nabla c = D\nabla^2 c. \tag{26}$$

The above equations express the conservation of mass, momentum (Darcy's law) and species, with c denoting the concentration of fluid 2. Both μ and ρ are assumed to be known functions of c,

$$\mu=\mu(c), \quad \rho=\rho(c). \tag{27}$$

Following Tan and Homsy, we introduce the velocity, length, and time scales U, D/U, and D/U^2. Furthermore, by scaling viscosity, density, and pressure by μ_1, ρ_1, and $\mu_1 D$, respectively, we obtain the set of dimensionless equations,

$$\frac{\partial u}{\partial x} + \frac{\partial v}{\partial y} = 0, \tag{28}$$

$$\frac{\partial p}{\partial x}=-\mu(u+1)+G\rho\sin\theta, \tag{29}$$

$$\frac{\partial p}{\partial y}=-\mu v-G\rho\cos\theta, \tag{30}$$

$$\frac{\partial c}{\partial t}+u\frac{\partial c}{\partial x}+v\frac{\partial c}{\partial y}=\frac{\partial^2 c}{\partial x^2}+\frac{\partial^2 c}{\partial y^2}, \tag{31}$$

where

$$G=\frac{\rho_1 g}{\mu_1 U} \tag{32}$$

is a dimensionless parameter describing the relative importance of gravitational and viscous effects. This system of equations admits the base-state solution,

$$u_0(x,t)=0, \tag{33}$$

$$v_0(x,t)=-\frac{1}{\mu_0}\left[\eta(t)+G\rho_0(x,t)\cos\theta\right], \tag{34}$$

$$p_0(x,t)=\int^x\left[-\mu_0(\xi,t)+G\rho_0(\xi,t)\sin\theta\right]d\xi+y\eta(t), \tag{35}$$

$$c_0(x,t)=\frac{1}{2}\left[1+\operatorname{erfc}\left(\frac{x}{2\sqrt{t}}\right)\right], \tag{36}$$

$$\mu_0=\mu_0(c_0)=\mu_0(x,t), \tag{37}$$

$$\rho_0=\rho_0(c_0)=\rho_0(x,t), \tag{38}$$

where $\eta(t)$ is an arbitrary function of time only. The existence of $\eta(t)$ reflects the fact that there are infinitely many velocity profiles $v_0(x,t)$ resulting in base state solutions, a fact that first became obvious in Sec. II, where we found infinitely many combinations of V_1 and V_2. The actual $v_0(x,t)$ selected is determined by the imposed pressure gradient at infinity. Notice, also, that the base flow velocity profile $v_0(x,t)$ depends on the viscosity-concentration and the density-concentration relationships, which are, as yet, unspecified.

B. Stability analysis

We now introduce small perturbation quantities, denoted by primed variables, into the flow field. After subtracting the base flow and linearizing, we obtain a set of equations governing the evolution of these small perturbations,

$$\frac{\partial u'}{\partial x}+\frac{\partial v'}{\partial y}=0, \tag{39}$$

$$\frac{\partial p'}{\partial x}=-\mu'-\mu_0 u'+G\rho'\sin\theta, \tag{40}$$

$$\frac{\partial p'}{\partial y}=-\mu' v_0-\mu_0 v'-G\rho'\cos\theta, \tag{41}$$

$$\frac{\partial c'}{\partial t}+u'\frac{\partial c_0}{\partial x}+v_0\frac{\partial c'}{\partial y}=\frac{\partial^2 c'}{\partial x^2}+\frac{\partial^2 c'}{\partial y^2}, \tag{42}$$

$$\mu'=\frac{d\mu}{dc}c', \quad \rho'=\frac{d\rho}{dc}c'. \tag{43}$$

By eliminating p' and v' from the above equations and expanding the perturbations into Fourier modes with wave number k in the y direction,

$$(u',c')(x,y,t)=(\Phi,\Psi)(x,t)e^{iky}, \tag{44}$$

we obtain two coupled partial differential equations for Φ and Ψ,

$$\left(\frac{\partial^2}{\partial x^2}+\frac{1}{\mu_0}\frac{\partial\mu_0}{\partial x}\frac{\partial}{\partial x}-k^2\right)\Phi$$
$$=\left[\frac{1}{\mu_0}\frac{d\mu}{dc}\left(k^2+ik\frac{\partial v_0}{\partial x}+ikv_0\frac{\partial}{\partial x}\right)+\frac{1}{\mu_0}\frac{d^2\mu}{dc^2}\left(ikv_0\frac{\partial c_0}{\partial x}\right)\right.$$
$$+G\frac{1}{\mu_0}\frac{d\rho}{dc}\left(-k^2\sin\theta+ik\cos\theta\frac{\partial}{\partial x}\right)$$
$$\left.+G\frac{1}{\mu_0}\frac{d^2\rho}{dc^2}\left(ik\cos\theta\frac{\partial c_0}{\partial x}\right)\right]\Psi, \tag{45}$$

$$\left(\frac{\partial}{\partial t}-\frac{\partial^2}{\partial x^2}+k^2+ikv_0\right)\Psi=-\frac{\partial c_0}{\partial x}\Phi. \tag{46}$$

We now employ the QSSA, thereby following Tan and Homsy,[4] who also give a brief discussion of the validity of this approach. In essence, the QSSA treats the base flow as time independent, i.e., as being frozen at time t_0. We then assume that perturbations grow or decay exponentially at a quasisteady rate,

$$(\Phi,\Psi)(x,t)=(\phi,\psi)(x,t_0)e^{\sigma(t_0)t}, \tag{47}$$

where ϕ, ψ, and σ are complex valued. The real part of the eigenvalue, σ_r, is the growth rate of the perturbations while $-\sigma_i/k$ is the phase speed of the traveling waves.

Equations (45) and (46) are then reduced to ordinary differential equations, yielding the eigensystem

$$\left(D^2+\frac{1}{\mu_0}\frac{d\mu_0}{dx}D-k^2\right)\phi$$
$$=\left[\frac{1}{\mu_0}\frac{d\mu}{dc}\left(k^2+ik\frac{dv_0}{dx}+ikv_0D\right)+\frac{1}{\mu_0}\frac{d^2\mu}{dc^2}\left(ikv_0\frac{dc_0}{dx}\right)\right.$$
$$+G\frac{1}{\mu_0}\frac{d\rho}{dc}\left(-k^2\sin\theta+ik\cos\theta D\right)$$
$$\left.+G\frac{1}{\mu_0}\frac{d^2\rho}{dc^2}\left(ik\cos\theta\frac{dc_0}{dx}\right)\right]\psi, \tag{48}$$

$$(D^2-\sigma-k^2-ikv_0)\psi=\frac{dc_0}{dx}\phi, \tag{49}$$

where $D\equiv d/dx$. The boundary conditions that u' and c' vanish at infinity become

$$\phi,\psi\to 0, \quad \text{as } x\to\pm\infty. \tag{50}$$

We are interested in determining the eigenvalue relation $\sigma(k)$ for various base state profiles in order to analyze the stability characteristics of the flow.

C. Viscosity and density relationships

To solve Eqs. (48) and (49), we have to know the functional dependence of viscosity and density on the concentration. These relationships will strongly influence the dynamics of the flow. In particular, when these functional forms are different, one can obtain situations in which density effects and viscosity effects dominate in different parts of the mixed region, thereby introducing different scales into the problem. For example, it appears possible to obtain a local region unstable to the viscous fingering mechanism embedded in a flow field globally stabilized by density effects.

Here we assume the simple relationships,

$$\mu(c)=e^{Rc}, \quad \rho(c)=e^{Sc}. \tag{51}$$

Equations (48) and (49) then become

$$\left(D^2+R\frac{dc_0}{dx}D-k^2\right)\phi$$

$$=\left(k^2(R-GSe^{(S-R)c_0}\sin\theta)+ikGS(S-R)e^{(S-R)c_0}\right.$$

$$\left.\times\cos\theta\frac{dc_0}{dx}+ik(Rv_0+GSe^{(S-R)c_0}\cos\theta)D\right)\psi, \tag{52}$$

$$(D^2-\sigma-k^2-ikv_0)\psi=\frac{dc_0}{dx}\phi, \tag{53}$$

where the base state profiles c_0 and v_0 are given by

$$c_0(x,t_0)=\frac{1}{2}\left[1+\operatorname{erfc}\left(\frac{x}{2\sqrt{t_0}}\right)\right], \tag{54}$$

$$v_0(x,t_0)=-e^{-Rc_0}[\eta(t_0)+G\cos\theta e^{Sc_0}], \tag{55}$$

and ϕ and ψ are subject to the boundary conditions,

$$\phi,\psi\to 0, \quad \text{as } x\to\pm\infty. \tag{56}$$

Notice that $\sigma(k)$ depends parametrically on R, S, G, θ, $c_0(x,t_0)$, and $v_0(x,t_0)$. The analytical solution to this system at time $t=0$ is presented next. For times $t>0$, a numerical solution is required. In the following section we discuss our approach to the numerical solution of Eqs. (52) and (53) for $t>0$ and the results we obtain from this investigation.

D. Solution at $t=0$

For the solution to Eqs. (52) and (53) at time $t=0$, we follow the procedure used by Tan and Homsy.[4] At $t=0$, the concentration and v-velocity base-state profiles are

$$c_0=\begin{cases}0, & x<0,\\ 1, & x>0,\end{cases} \tag{57}$$

$$v_0=\begin{cases}V_1, & x<0,\\ V_2, & x>0,\end{cases} \tag{58}$$

so that $dc_0/dx=\delta(x)$. Away from $x=0$, Eqs. (52) and (53) become

$$(D^2-k^2)\phi^-=[k^2(R-GS\sin\theta)+ik(RV_1+GS\cos\theta)D]\psi^-, \tag{59}$$

$$(D^2-\sigma-k^2-ikV_1)\psi^-=0, \tag{60}$$

for $x<0$, and

$$(D^2-k^2)\phi^+=[k^2(R-GSe^{(S-R)}\sin\theta)+ik(RV_2+GSe^{(S-R)}\cos\theta)D]\psi^+, \tag{61}$$

$$(D^2-\sigma-k^2-ikV_2)\psi^+=0, \tag{62}$$

for $x>0$. Applying the boundary conditions,

$$\phi,\psi\to 0, \quad \text{as } x\to\pm\infty, \tag{63}$$

we obtain the solution for $x\neq 0$,

$$\psi^+=z_1e^{-\alpha x}, \tag{64}$$

$$\phi^+=z_2e^{-kx}+z_3e^{-\alpha x}, \tag{65}$$

$$\psi^-=\mathscr{Z}_1e^{\beta x}, \tag{66}$$

$$\phi^-=\mathscr{Z}_2e^{kx}+\mathscr{Z}_3e^{\beta x}, \tag{67}$$

where

$$\alpha^2=\sigma+k^2+ikV_2, \tag{68}$$

$$\beta^2=\sigma+k^2+ikV_1, \tag{69}$$

and

$$z_3=\frac{z_1}{(\alpha^2-k^2)}[k^2(R-GSe^{(S-R)}\sin\theta)-ik\alpha(RV_2+GSe^{(S-R)}\cos\theta)], \tag{70}$$

$$\mathscr{Z}_3=\frac{\mathscr{Z}_1}{(\beta^2-k^2)}[k^2(R-GS\sin\theta)+ik\beta(RV_1+GS\cos\theta)]. \tag{71}$$

The conditions of continuous perturbation concentration, u velocity, and pressure at the interface further require

$$\mathscr{Z}_1=z_1, \tag{72}$$

$$\mathscr{Z}_2=\frac{kz_1}{(1+e^R)}\left[-R\left(\frac{1}{\beta}+\frac{e^R}{\alpha}\right)+GS\sin\theta\left(\frac{1}{\beta}+\frac{e^S}{\alpha}\right)+\frac{e^R(\alpha-k)}{\alpha k(\alpha^2-k^2)}A_2-\frac{(k+\beta e^R)}{\beta k(\beta^2-k^2)}A_1\right], \tag{73}$$

$$z_2=\frac{kz_1}{(1+e^R)}\left[-R\left(\frac{1}{\beta}+\frac{e^R}{\alpha}\right)+GS\sin\theta\left(\frac{1}{\beta}+\frac{e^S}{\alpha}\right)-\frac{(ke^R+\alpha)}{\alpha k(\alpha^2-k^2)}A_2+\frac{(\beta-k)}{\beta k(\beta^2-k^2)}A_1\right], \tag{74}$$

where

$$A_1=[k^2(R-GS\sin\theta)+ik\beta(RV_1+GS\cos\theta)], \tag{75}$$

$$A_2=[k^2(R-GSe^{(S-R)}\sin\theta)$$
$$-ik\alpha(RV_2+GSe^{(S-R)}\cos\theta)]. \quad (76)$$

Integrating Eq. (53) at time $t=0$ over the interface,

$$\int_{0^-}^{0^+}(D^2-\sigma-k^2-ikv_0)\psi\,dx=\int_{0^-}^{0^+}\delta(x)\phi\,dx, \quad (77)$$

yields a relation for σ,

$$f(\sigma)=(\alpha+\beta)+\frac{k}{(1+e^R)}\left[-R\left(\frac{1}{\beta}+\frac{e^R}{\alpha}\right)+GS\right.$$
$$\left.\times\sin\theta\left(\frac{1}{\beta}+\frac{e^S}{\alpha}\right)+\frac{e^RA_2}{\alpha k(\alpha+k)}+\frac{A_1}{\beta k(\beta+k)}\right]=0, \quad (78)$$

where

$$\alpha^2=\sigma+k^2+ikV_2, \quad (79)$$

$$\beta^2=\sigma+k^2+ikV_1, \quad (80)$$

$$A_1=[k^2(R-GS\sin\theta)+ik\beta(RV_1+GS\cos\theta)], \quad (81)$$

$$A_2=[k^2(R-GSe^{(S-R)}\sin\theta)$$
$$-ik\alpha(RV_2+GSe^{(S-R)}\cos\theta)]. \quad (82)$$

We can solve Eq. (78) for $\sigma(k)$ analytically when $V_1=V_2$. According to Eq. (55), V_1 and V_2 are given by

$$V_1=-(\eta+G\cos\theta), \quad (83)$$

$$V_2=-e^{-R}(\eta+G\cos\theta e^S), \quad (84)$$

yielding

$$V_1=V_2=-G\cos\theta\frac{(1-e^S)}{(1-e^R)}, \quad (85)$$

when $\eta=G\cos\theta(e^R-e^S)/(1-e^R)$. Then

$$f(\sigma)=2\alpha-\frac{k\tilde{R}}{\alpha}+\frac{k^2\tilde{R}}{\alpha(\alpha+k)}+i\frac{k\tilde{Q}}{(\alpha+k)}=0, \quad (86)$$

where

$$\tilde{R}=R-GS\sin\theta\frac{(1+e^S)}{(1+e^R)}, \quad (87)$$

$$\tilde{Q}=G(S-R)\cos\theta\frac{(1-e^S)}{(1+e^R)}, \quad (88)$$

resulting in

$$\sigma(k)=\frac{k}{2}[(\tilde{R}-k)-i(\tilde{Q}+2V_1)-\sqrt{k^2+2k(\tilde{R}-i\tilde{Q})}]. \quad (89)$$

The restriction $V_1=V_2$ does not necessarily produce a constant v-velocity base state at times $t>0$. From Eq. (55) we see that a constant v_0 requires either $G=0$, $S=0$, $R=S$, or $\theta=\pi/2$. In each of these cases, $\tilde{Q}=0$, and we can easily extract the growth rate,

$$\sigma_r(k)=\frac{k}{2}[(\tilde{R}-k)-\sqrt{k^2+2k\tilde{R}}]$$
$$=\frac{k}{2}\left[\left(R-GS\sin\theta\frac{(1+e^S)}{(1+e^R)}-k\right)\right.$$
$$\left.-\sqrt{k^2+2k\left(R-GS\sin\theta\frac{(1+e^S)}{(1+e^R)}\right)}\right] \quad (90)$$

and

$$\sigma_i(k)=-kv_0=kG\cos\theta\frac{(1-e^S)}{(1-e^R)}. \quad (91)$$

Equation (90) indicates that there will be growing modes for $\tilde{R}>0$, with the cutoff wave number, $k=\tilde{R}/4$. Therefore when v_0 is constant, the criterion for instability is

$$\tilde{R}=R-GS\sin\theta\frac{(1+e^S)}{(1+e^R)}>0, \quad (92)$$

which in dimensional form is

$$U(\mu_1+\mu_2)(\ln\mu_2-\ln\mu_1)-g\sin\theta(\rho_1+\rho_2)$$
$$\times(\ln\rho_2-\ln\rho_1)>0. \quad (93)$$

For the no-gravity case, $G=0$ or $S=0$, and $v_0=0$, we obtain the growth rate found by Tan and Homsy,[4]

$$\sigma=\sigma_r=(k/2)(R-k-\sqrt{k^2+2kR}), \quad (94)$$

indicating that the flow is unstable whenever the more viscous fluid is displaced by the less viscous fluid, i.e., $R>0$.

When the viscosity and density have the same functional form ($R=S$) there is a constant tangential velocity base state,

$$v_0=-G\cos\theta, \quad (95)$$

and the criterion for instability becomes

$$R(1-G\sin\theta)>0. \quad (96)$$

Figure 2(a) shows the initial growth rates in this case for $R=S=3$, $G=1$, and various angles of inclination θ. For a vertical interface ($\theta=0$), we can see from Eq. (90) that we obtain the Tan and Homsy result (94), even though the two fluids have different densities and a nonzero tangential velocity. As θ increases from zero to $\pi/2$, $(1-G\sin\theta)$ decreases, and the flow configuration becomes more stable as gravity is aligned with the normal displacement velocity and is directed from the lighter fluid, fluid 1, to the heavier fluid 2. As θ decreases from zero to $-\pi/2$, $(1-G\sin\theta)$ increases, and the growth rate increases. Here the flow configuration becomes more unstable as gravity is directed from the heavier fluid to the lighter fluid. Since $G=1$ for the results shown in Fig. 2(a), the perturbations are neutrally stable at time $t=0$ for $\theta=\pi/2$.

When the interface is horizontal ($\theta=\pi/2$) and $v_0=0$, we get instability when

$$R-GS\frac{(1+e^S)}{(1+e^R)}>0. \quad (97)$$

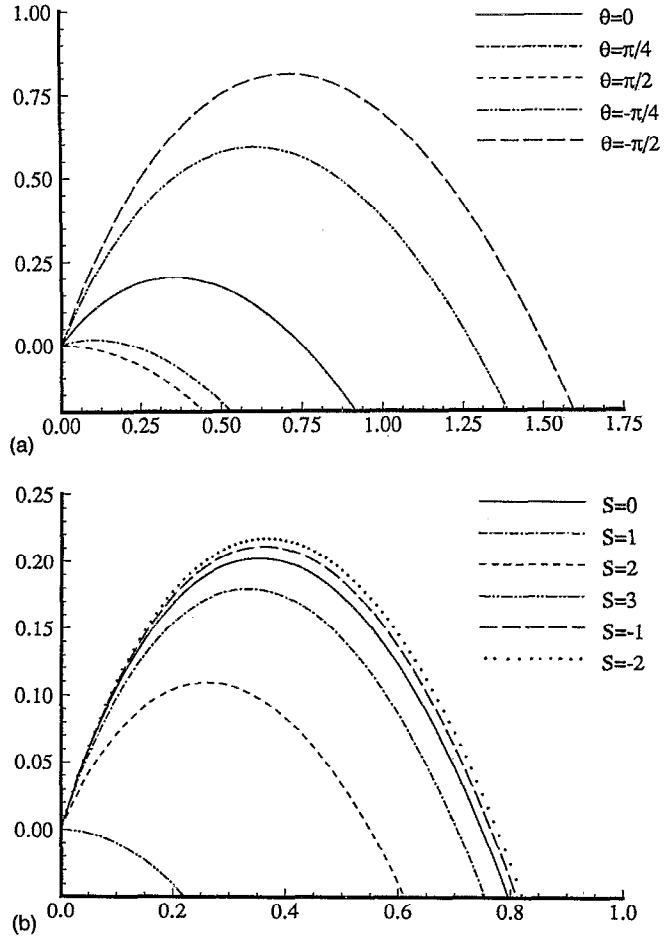

FIG. 2. Effect of density stratification on the initial growth rate for $V_1=V_2$. (a) $R=S=3$, $G=1$, $v_0=-G\cos\theta$. A vertical interface ($\theta=0$) yields the same growth rate as Tan and Homsy find when $v_0=0$. Since $\rho_1<\rho_2$, the stability is increased when $0<\theta<\pi/2$, since gravity is directed from fluid 1 to fluid 2 while for $-\pi/2<\theta<0$, the configuration is more unstable. (b) Horizontal interface ($\theta=\pi/2$), $R=3$, $G=1$, and $v_0=0$. Here $S=0$ corresponds to the no-gravity case ($\rho_1=\rho_2$). Since gravity is directed from fluid 1 to fluid 2, the fluids are stably stratified when $S>0$ ($\rho_1<\rho_2$) and unstably stratified when $S<0$.

Figure 2(b) shows the growth rate for $\theta=\pi/2$, $R=3$, and $G=1$ for various values of S. For $G=1$, Eq. (97) indicates that there will be unstable modes for $S<R$. Here $S=0$ corresponds to the no-gravity case since $\rho_1=\rho_2$. For $S<0$ the growth rate increases since $\rho_1>\rho_2$ and gravity is directed from fluid 1 toward fluid 2, while $0<S<R$ corresponds to a more stable configuration with gravity directed from the lighter fluid to the heavier fluid.

For $V_1\neq V_2$, $\sigma(k)$ is obtained from Eq. (78) using a standard iterative root-finding technique. For these more general v-velocity base-state profiles, we find that although the cutoff wave number and maximum growth rate vary with (V_1,V_2), we always get a band of unstable wave numbers when Eq. (92) is satisfied. This suggests that the instability criterion derived for constant v_0,

$$R-GS\sin\theta\frac{(1+e^S)}{(1+e^R)}>0, \tag{98}$$

also holds for more general v-velocity base states. This will be illustrated in Sec. V, where we further discuss the influence of nonconstant tangential velocities on the stability of the flow.

V. NUMERICAL SOLUTION TO MISCIBLE STABILITY EQUATIONS

Tan and Homsy[4] and Yortsos and Zeybek[5] have solved eigenvalue problems similar to the system described by Eqs. (52) and (53) for the case where there are no tangential base-state velocities. Both of these studies used the shooting method to obtain the eigenvalues and eigenfunctions of the system. In this study we will, instead, use a Chebyshev spectral method (cf. Ref. 11). A mapping is used to map the physical domain $x=(-\infty,\infty)$ to the Chebyshev domain $\zeta=[-1,1]$, therefore a collocation method is implemented.

We are interested in obtaining the complete spectrum $\sigma(k)$ for various parameter sets (R,S,G,θ,c_0,v_0). Since c_0 is a step function for $t=0$, the method described here will only be used to compute the spectrum at times $t>0$ when the profiles are smooth.

A. Numerical method

The Chebyshev polynomials are defined on the interval $[-1,1]$, while the stability problem is defined on the domain $x=(-\infty,\infty)$. One way to handle this is by truncating the physical domain to $\hat{x}=[-L,L]$ and mapping this linearly onto $[-1,1]$. Although Zeybek and Yortsos (and presumably Tan and Homsy as well) use a truncated domain for their computations, there is no need for us to do this since we can map the infinite domain directly onto $[-1,1]$. To maintain spectral convergence of the scheme, we use the algebraic map,[11]

$$x=f^{-1}(\zeta)=a\frac{\zeta}{\sqrt{1-\zeta^2}}, \tag{99}$$

$$\zeta=f(x)=\frac{x}{\sqrt{a^2+x^2}}, \tag{100}$$

where a is the length scale of the map. Using expansions in Chebyshev polynomials to approximate $\phi(\zeta)$ and $\psi(\zeta)$,

$$\phi(x)=\phi[f^{-1}(\zeta)]=\sum_{k=0}^{N}\hat{\phi}_k T_k(\zeta), \tag{101}$$

$$\psi(x)=\psi[f^{-1}(\zeta)]=\sum_{k=0}^{N}\hat{\psi}_k T_k(\zeta), \tag{102}$$

we recast the system (52) and (53) as a complex generalized eigenvalue equation in the ζ coordinates,

$$P\varphi=\sigma Q\varphi, \tag{103}$$

at the Gauss–Lobatto collocation points,

$$\zeta_j=\cos(\pi j/N), \quad \text{for} \quad j=0,\ldots,N. \tag{104}$$

Here P and Q are $(2N+2)\times(2N+2)$ matrices, and $\varphi=(\phi_0,\ldots,\phi_N,\psi_0,\ldots,\psi_N)$. The boundary conditions $(\phi,\psi)=(0,0)$ at $\zeta=\pm1$ are implemented by modifying the matrices P and Q,[12]

$$\hat{P}_{ij}=\begin{cases}\delta_{ij}, & \text{for } i=0,N,N+1,2N+1,\\ P_{ij}, & \text{otherwise,}\end{cases} \tag{105}$$

and

$$\hat{Q}_{ij}=\begin{cases}1, & \text{for } i=j=N+2,...,2N,\\ 0, & \text{otherwise,}\end{cases} \tag{106}$$

so that $\phi_{0,N}=0$ and $\psi_{0,N}=0$ are enforced directly. This new system,

$$\hat{P}\varphi=\sigma\hat{Q}\varphi, \tag{107}$$

is then solved using a standard QZ factorization routine. The results presented in the next section were computed using $N=48$ Chebyshev modes for $t>1$ and $N=96$ modes for $t<1$, and a map length scale of $a=10$ for $k>0.1$ and $a=25$ for $k<0.1$, yielding converged values for σ to six significant figures.

B. Results

We begin by first comparing our results with those of Tan and Homsy for the no-gravity case.[4] For $G=0$ (or $S=0$) and no tangential velocity, $v_0=0$, the equations simplify to those solved by Tan and Homsy in which σ is real valued,

$$\left(D^2+R\frac{dc_0}{dx}D-k^2\right)\phi=k^2R\psi, \tag{108}$$

$$(D^2-\sigma-k^2)\psi=\frac{dc_0}{dx}\phi. \tag{109}$$

Figures 3(a) and 3(b) show the dispersion relation for $R=2$ and $R=3$, respectively, at times $t=5,10,20$ compared with the results of Tan and Homsy. We see that the results agree very well. Dispersion provides a cutoff wave number and the spreading of the interface produces a growth rate that decays with time while shifting the cutoff wave number and most unstable mode to longer wavelengths. These general features are seen in all the cases we have investigated in which tangential velocities and gravitational forces also exist.

Next we consider the case in which a constant tangential velocity, v_0, is present. We take $R=S$ and $\eta=0$ so that

$$v_0=-G\cos\theta. \tag{110}$$

The eigensystem then becomes

$$\left(D^2+R\frac{dc_0}{dx}D-k^2\right)\phi=[k^2R(1-G\sin\theta)]\psi, \tag{111}$$

$$(D^2-\sigma-k^2-ikv_0)\psi=\frac{dc_0}{dx}\phi. \tag{112}$$

Since the first equation is real valued, the second equation yields

$$\sigma_i=-kv_0, \tag{113}$$

indicating that the waves travel with the velocity of the fluid as expected. For fixed R, the growth rate, σ_r, decreases to zero as $(1-G\sin\theta)\to 0$ and increases as $(1-G\sin\theta)$ increases. Figure 4 plots growth rates for $R=S=3$, $G=1$, and various values of θ, at time $t=5$. For $\theta=0$ when the interface is vertical, we obtain the same growth rate as in the no-gravity $v_0=0$ case. The constant tangential velocity does not affect the growth rate of the perturbations but does allow them to travel with the fluid velocity. As we found in Sec. IV D for time $t=0$, the growth

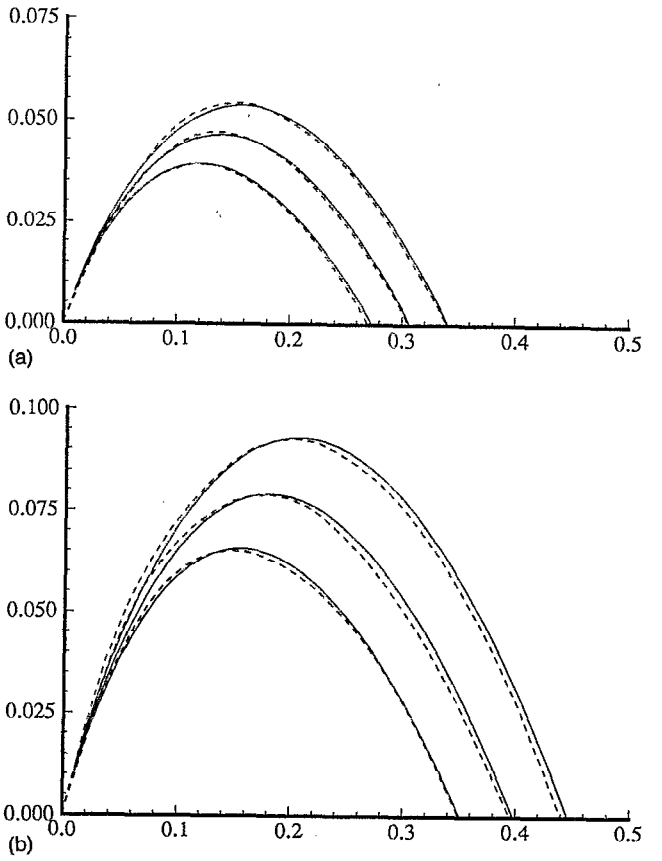

FIG. 3. Growth rate comparison with the results of Tan and Homsy (dashed line) corresponding to $G=0$ and no tangential velocity, $v_0=0$, at times $t=5$, 10, and 20; (a) $R=2$, (b) $R=3$.

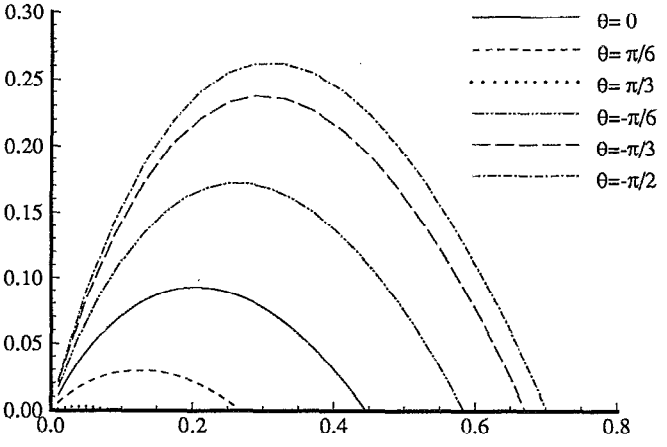

FIG. 4. Growth rate versus wave number for constant tangential velocity, $v_0=-G\cos\theta$, and various angles of inclination. Here $R=S=3$, $G=1$, and $t=5$. A vertical interface ($\theta=0$) yields the same growth rate as the no-gravity $v_0=0$ case. Since $\rho_1<\rho_2$, for $0<\theta<\pi/2$, the fluids are stably stratified with respect to buoyancy forces, while for $-\pi/2<\theta<0$, the fluids are unstably stratified.

rate varies with θ due to the density stratification. As the angle of inclination increases to $\theta=\pi/2$, the flow configuration becomes more stable since gravity is directed from the lighter fluid, fluid 1, to the heavier fluid, fluid 2. As θ decreases from zero to $-\pi/2$, the growth rate increases, since gravity is directed from the heavier fluid to the lighter fluid.

We now consider a case in which a tangential velocity shear exists at the interface. If we let $S=0$ (i.e., $\rho_1=\rho_2$), the eigensystem becomes

$$\left(D^2+R\frac{dc_0}{dx}D-k^2\right)\phi=(k^2R+ikRv_0D)\psi, \tag{114}$$

$$(D^2-\sigma-k^2-ikv_0)\psi=\frac{dc_0}{dx}\phi. \tag{115}$$

Since both fluids have the same density, the equations are independent of the angle of inclination θ and the parameter G. The induced v-velocity base state is

$$v_0=-e^{-Rc_0}(\eta+G\cos\theta), \tag{116}$$

where η is arbitrary. Growth rates for $R=3$ and various tangential base-state velocities at time $t=5$ are shown in Fig. 5(a). As $|V_1-V_2|=(1-e^{-R})|V_1|$ increases, the growth rate and the range of unstable wave numbers decreases, indicating that a tangential velocity difference across the interface has a stabilizing effect. Even though the stabilizing effect can be substantial, our analysis for time $t=0$ (Sec. IV D) indicates that a tangential velocity shear cannot completely stabilize a flow that is otherwise unstable. Figure 6 plots the initial growth rates for very strong tangential shearing velocities, obtained by solving Eq. (78) for this case ($S=0$) and a more general parameter set. Since we always get a band of unstable wave numbers, the criterion for instability we derived in the no-shear case [Eq. (92)] still holds. The influence of tangential velocity shear on the growth rate is in marked contrast to the results for the immiscible case with and without surface tension, for which the growth rate is independent of the tangential velocities V_1 and V_2. The physical mechanism for this will be discussed in more detail below. Furthermore, the phase speed, $-\sigma_i/k$, in immiscible displacement is given by the viscosity-weighted average of V_1 and V_2. This is also not the case for miscible flow, as shown in Fig. 5(b), where the viscosity-weighted average result, $\sigma_i=-k(\mu_1V_1+\mu_2V_2)/(\mu_1+\mu_2)$, is also plotted for comparison. We see that the magnitude of the phase speed increases as the strength of the tangential shear increases but that the phase speed is not approximated by the viscosity-weighted average of V_1 and V_2. Clearly, the phase speed of the traveling waves has some other functional dependence on the tangential velocities and viscosities of the two phases, and also depends, as illustrated later in this section, on the densities of the fluids. The temporal evolution of the growth rate is depicted in Fig. 7 for $k=0.2$. The numerical results obtained for $t>0$ asymptotically approach the analytical solution for $t=0$, which is plotted as well. For times $t>1$ we see that for all cases the growth rate decreases with time due to the dispersive

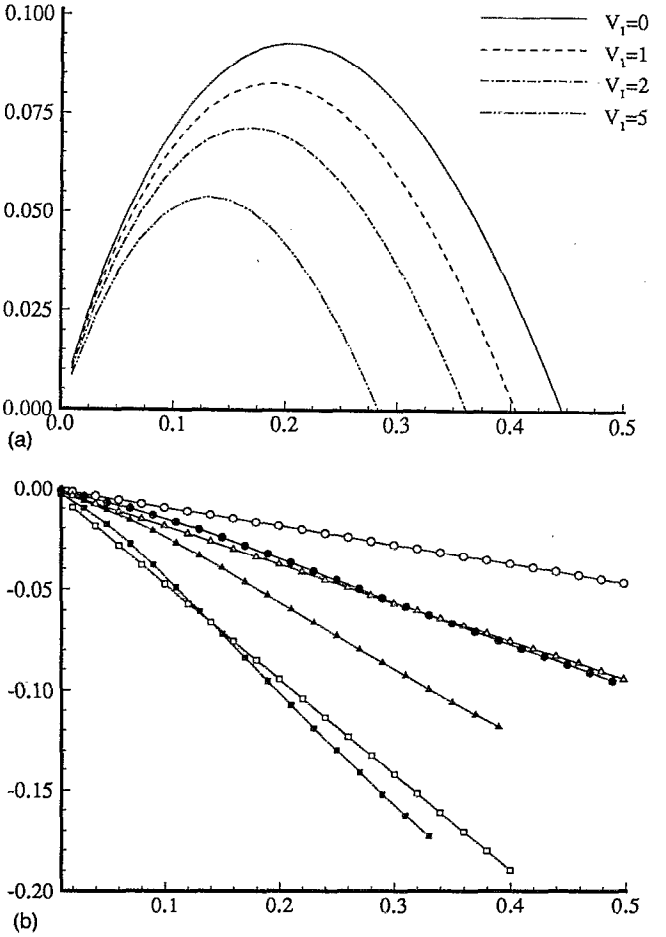

FIG. 5. Effect of tangential velocity shear on growth rate and phase speed for two fluids of the same density. Here $S=0$, $R=3$, $t=5$, $|V_1|=1,2,5$, and $V_2=e^{-R}V_1$; (a) growth rate versus wave number showing increased stabilization as $|V_1-V_2|$ increases. (b) σ_i versus wave number. Solid symbols correspond to the miscible QSSA results; hollow symbols correspond to viscosity-weighted average phase speed. $\bigcirc, V_1=1$; $\triangle, V_1=2$; $\square, V_1=5$.

spreading of the front. However, when a strong tangential shear is present, there is initially a short period of increasing growth rate, resulting in a maximum at time $t>0$. We remark that the QSSA employed in this analysis approximates the actual growth rate only for large times when the base-state flow changes slowly, and therefore the short period of increasing growth rate with time illustrated here may or may not have any physical relevance.

The stabilizing effect of tangential shearing velocity can be understood by examining the perturbation vorticity equation. The equations governing the perturbation pressure are

$$\frac{\partial p'}{\partial x}=-\mu'-\mu_0u'+G\rho'\sin\theta, \tag{117}$$

$$\frac{\partial p'}{\partial y}=-\mu'v_0-\mu_0v'-G\rho'\cos\theta. \tag{118}$$

By eliminating the pressure, we obtain the equation for the perturbation vorticity,

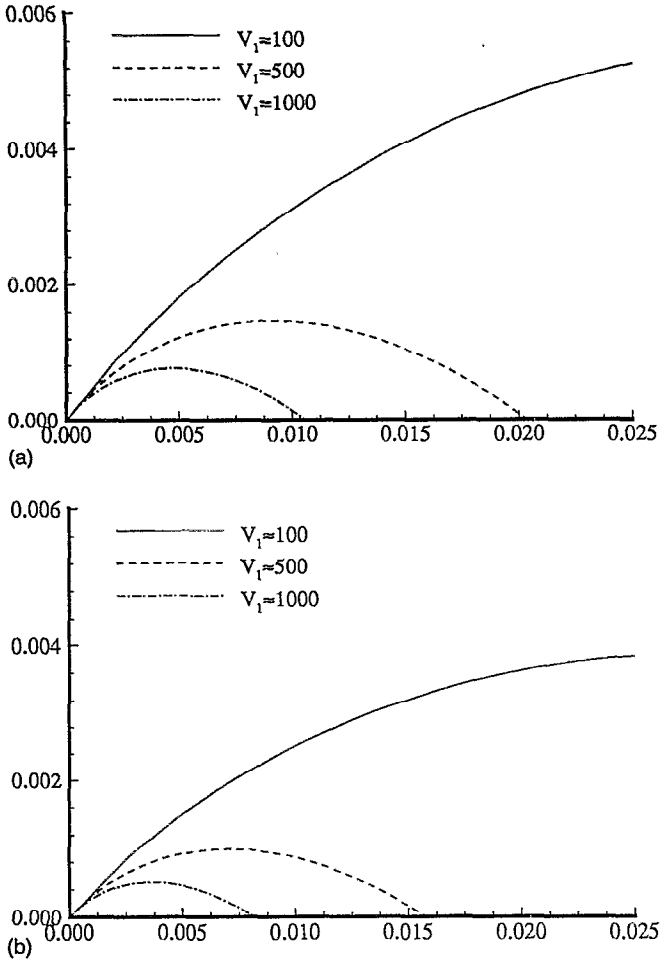

FIG. 6. Initial growth rates for strong tangential shearing velocities. A band of unstable wave numbers persists, indicating that the tangential shear cannot completely stabilize the flow. (a) $S=0$, $R=3$, $|V_1-V_2|=\eta(e^{-R}-1)$, and $\eta=100$, 500, 1000. (b) $S=2$, $R=3$, $G=1$, $\theta=\pi/6$, $|V_1-V_2|=\eta(e^{-R}-1)+G\cos\theta(e^{S-R}-1)$, and $\eta=100$, 500, 1000.

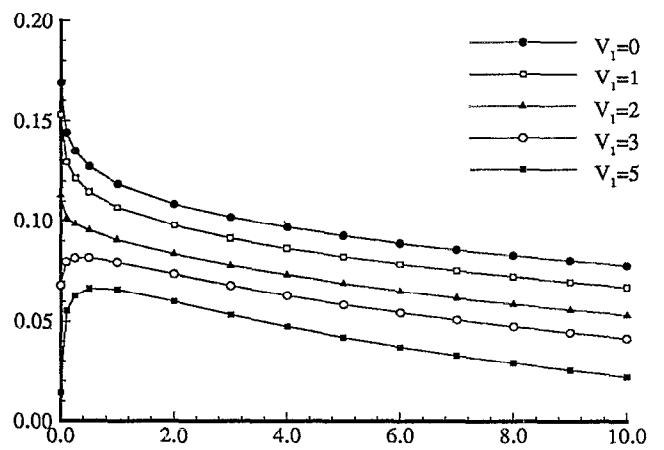

FIG. 7. Growth rate versus time for $S=0$, $R=3$, $k=0.2$, $|V_1|=0,1,2,3,5$, and $V_2=e^{-R}V_1$. The analytical solution at $t=0$ is plotted with the numerical solution for $t=0.1$, 0.25, 0.5, 1, 2,...,10. For strong tangential shearing velocities, the maximum growth rate shifts away from $t=0$.

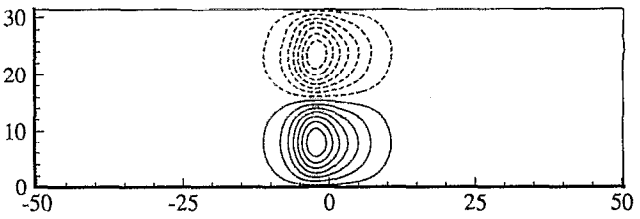

FIG. 8. Total vorticity, $\omega'=R[(\partial c'/\partial y)-(\partial c_0/\partial x)v']$, for the no-shear case, $v_0(x)=0$. Here $R=3$, $S=0$, $t=5$, and $k=0.2$.

$$\omega'=\frac{1}{\mu_0}\left(\frac{\partial\mu'}{\partial y}-\frac{\partial\mu_0}{\partial x}v'-\frac{\partial\mu'}{\partial x}v_0-\mu'\frac{\partial v_0}{\partial x}-G\cos\theta\frac{\partial\rho'}{\partial x}\right.$$
$$\left.-G\sin\theta\frac{\partial\rho'}{\partial y}\right), \tag{119}$$

or, in terms of the parameters R and S,

$$\omega'=R\left(\frac{\partial c'}{\partial y}-\frac{\partial c_0}{\partial x}v'-\frac{\partial c'}{\partial x}v_0-c'\frac{\partial v_0}{\partial x}\right).$$
$$-GSe^{(S-R)c_0}\left(\cos\theta\frac{\partial c'}{\partial x}+\sin\theta\frac{\partial c'}{\partial y}\right). \tag{120}$$

For comparison with the preceding results, consider the case of constant density ($S=0$), so that

$$\omega'=R\left(\frac{\partial c'}{\partial y}-\frac{\partial c_0}{\partial x}v'-\frac{\partial c'}{\partial x}v_0-c'\frac{\partial v_0}{\partial x}\right), \tag{121}$$

where the last two terms are due to the presence of a tangential shear. For the representative set of parameter values $R=3$, $t=5$, and $k=0.2$, the vorticity in the case of no shearing velocity, $v_0(x)=0$, is shown in Fig. 8. We can compare this with the vorticity field produced when a shearing velocity does exist. Figure 9(a) shows the contributions from the first two terms of Eq. (121) for the tangential velocity base state $v_0=2e^{Rc_0}$. While the tangential shear clearly breaks the symmetry present in the no-shear case, its effect is merely a slight deformation of the vorticity contours, which cannot be the cause of the drastic growth rate reduction described above. Even inclusion of the shear-related term,

$$-\frac{1}{\mu_0}\mu'\frac{\partial v_0}{\partial x}=-Rc'\frac{\partial v_0}{\partial x}, \tag{122}$$

which represents vorticity slightly out of phase with the contribution of the first two terms, results only in a slight shift of the contours in the direction parallel to the interface [Fig. 9(b)], so that it cannot account for the increased stabilization either. However, by also including the term

$$-\frac{1}{\mu_0}\frac{\partial\mu'}{\partial x}v_0=-R\frac{\partial c'}{\partial x}v_0, \tag{123}$$

we notice that the previous dipolelike structure of the overall vorticity changes to a less unstable quadrupolelike structure, representing the apparent reason for the increased stabilization of the flow [Fig. 9(c)]. Separate inspection of the expressions $-R(\partial c'/\partial x)$ and v_0 further

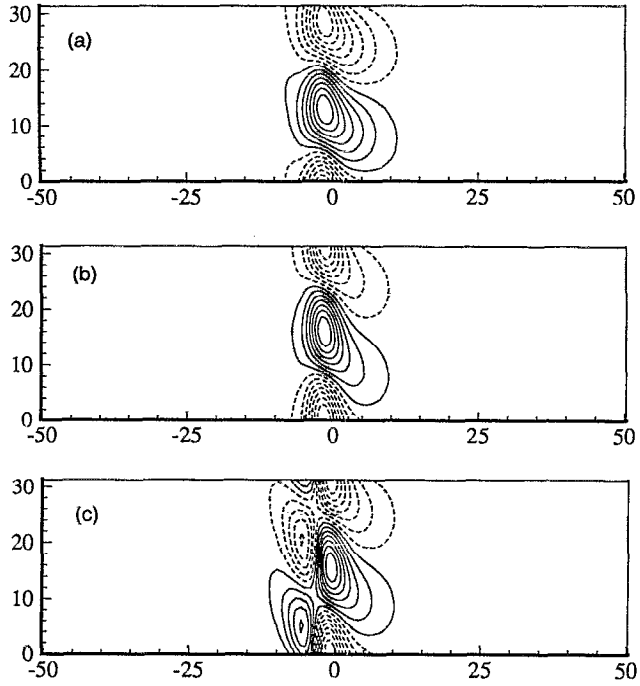

FIG. 9. Separate vorticity contributions for flow with tangential shearing velocity, $v_0(x) = 2e^{-Rc_0}$. Here $R=3$, $S=0$, $t=5$, $k=0.2$. (a) $\omega_a'=R[(\partial c'/\partial y)-(\partial c_0/\partial x)v']$. (b) $\omega_b'=R[(\partial c'/\partial y)-(\partial c_0/\partial x)v' -c'(\partial v_0/\partial x)]$. (c) Total vorticity, $\omega'=R[(\partial c'/\partial y)-(\partial c_0/\partial x)v' -(\partial c'/\partial x)v_0-c'(\partial v_0/\partial x)]$.

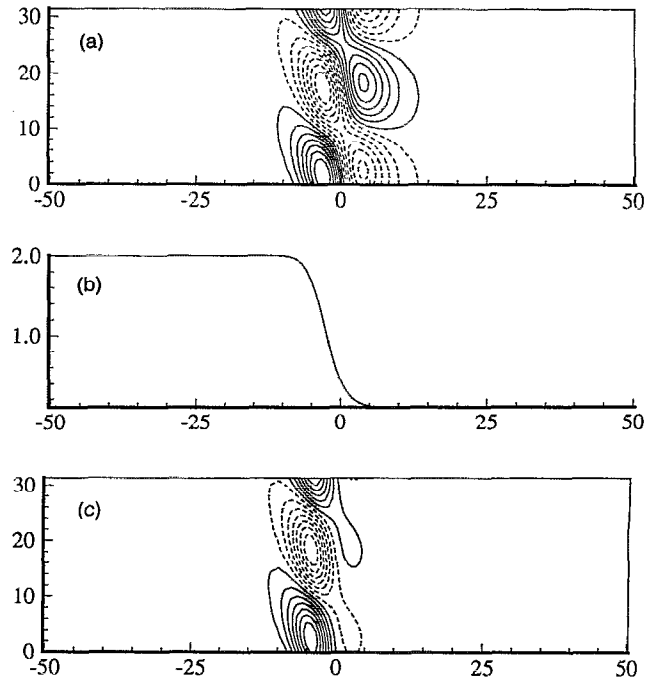

FIG. 10. Term responsible for quadrupole vorticity structure. Here $v_0(x) = 2e^{-Rc_0}$, $R=3$, $S=0$, $t=5$, and $k=0.2$. A combination of (a) $-R(\partial c'/\partial x)$ and (b) v_0, produces a dipolelike structure on the upstream side of the interface. (c) $-R(\partial c'/\partial x)v_0$.

illustrates the role of this term (Fig. 10). While $-R(\partial c'/\partial x)$ itself exhibits a quadrupolelike structure with maxima and minima on opposite sides of the y axis, weighting with the base-flow velocity profile v_0 [Fig. 10(b)] effectively annihilates the contribution from $y>0$, thereby leaving a dipolelike distribution centered on the upstream side of the displacement front [Fig. 10(c)]. This field, when added to remaining terms, results in the quadrupole structure of the overall vorticity field. It is this strong variation of $v_0(x)$ across the concentration front, i.e., the strong tangential shear, that is ultimately responsible for the increased stabilization of the flow. Furthermore, the above discussion also explains the fundamental difference between miscible and immiscible displacements. In the immiscible case, the front remains sharp while the miscible flow case has a widening front. It is the dispersive spreading of the miscible front that supports the quadrupolelike vorticity structure. This structure cannot emerge in the concentrated vorticity sheet produced by immiscible displacement.

We have seen that the presence of tangential velocity shear at the interface has a stabilizing effect for two fluids of the same density. When the phases have different densities, the growth rate is further reduced or enhanced when the fluids are stably or unstably stratified with respect to buoyancy forces. For simplicity, consider a horizontal interface, with **g** aligned with the normal displacement velocity ($\theta=\pi/2$), resulting in the equations

$$\left(D^2+R\frac{dc_0}{dx}D-k^2\right)\phi=[k^2(R-GSe^{(S-R)c_0}) +ikRv_0D]\psi, \tag{124}$$

$$(D^2-\sigma-k^2-ikv_0)\psi=\frac{dc_0}{dx}. \tag{125}$$

with v-velocity base state,

$$v_0=-e^{-Rc_0}\eta. \tag{126}$$

We vary the density difference by holding $G=(\rho_1 g)/(\mu_1 U)$ fixed (i.e., ρ_1 fixed) and varying S (varying $\rho_2=e^S\rho_1$). Figure 11(a) plots growth rates for $R=3$, $G=1$, and $V_1=1$ ($V_2=e^{-R}$) at time $t=5$ for various values of S. As we found in Sec. IV D for $t=0$, when $S>0$ the growth rate is reduced since gravity is directed from the lighter fluid, fluid 1, to the heavier fluid, fluid 2. Conversely, for $S<0$, there is an increased growth rate since fluid 1 is heavier than fluid 2. Plots of σ_i vs k in Fig. 11(b) show that the phase speed increases as S decreases. If the two fluids have the same density, we denote the phase speed of the perturbations by γ^*. For $\rho_1<\rho_2$ ($S>0$) we get a slower wave speed, $\gamma<\gamma^*$, while for $\rho_1>\rho_2$ ($S<0$) a faster wave speed, $\gamma>\gamma^*$, results. Since $V_1>V_2$ we find that although, in general, the waves tend to travel with the more viscous phase, there is also a tendency for the perturbations to travel with the denser fluid. This suggests that the phase speed may be weakly dependent on the density-weighted average of V_1 and V_2.

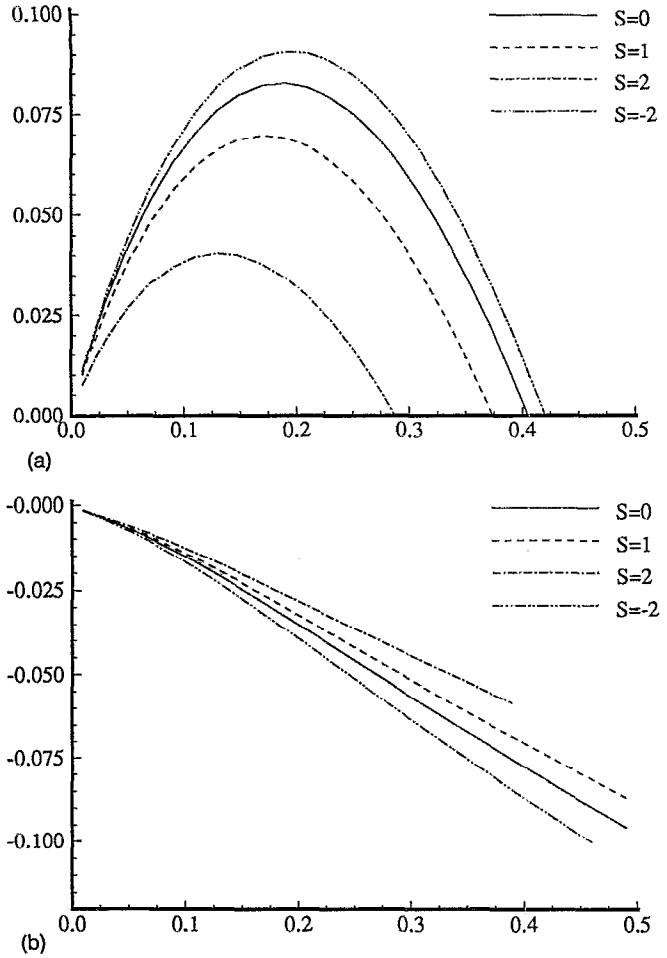

FIG. 11. Effect of density stratification in addition to tangential velocity shear. Here $R=3$, $G=1$, $t=5$, $|V_1|=1$, $V_2=e^{-R}$, and $S=2,1,0,-2$; (a) growth rate versus wave number. For $S>0$, the fluids have a stable density stratification, yielding a reduced growth rate. For $S<0$, the unstable density stratification enhances the growth rate. (b) σ_i versus wave number showing increasing phase speed as S increases.

VI. CONCLUSIONS

We have extended previous studies on the stability of two-phase porous media flows by allowing for the simultaneous presence of velocity components both normal and tangential to the interface. We find that the traveling waves observed experimentally and analytically by Zeybek and Yortsos[7,8] for the case of immiscible fluids and tangential velocities only, can grow or decay under the additional influence of a normal displacement velocity, in accordance with the well-known viscous fingering instability. For the case of immiscible fluids, the growth rate of the waves is unaffected by the presence of tangential velocity components, while surface tension acts to stabilize the displacement process. Miscible fluids, however, display a fundamentally different behavior. Here, tangential shear increases the stability of the displacement process. We explain this unexpected effect by analyzing the perturbation vorticity equation, which exhibits a less unstable quadrupole structure instead of the dipole structure known from the classical case. This quadrupole structure is a result of a shearing tangential velocity profile across the finite thickness front, and explains why the increased stabilization cannot occur for the immiscible case, where a sharp front is maintained. Furthermore, we find that in the miscible displacement case, the phase speed of the waves is not given by the viscosity-weighted average of the tangential velocities, as it is in the immiscible case. The above findings lead us to conclude that miscible and immiscible two-phase porous media flows, which behave similarly in the absence of tangential velocities, might give rise to quite different nonlinear dynamics in the presence of tangential velocity components. Full nonlinear simulations are required to obtain further interesting insight of use for practical applications, such as reservoir modeling.

ACKNOWLEDGMENTS

We wish to thank Professors G. M. Homsy, T. Maxworthy, and Y. Yortsos for their helpful discussions.

We gratefully acknowledge support for this research by the National Science Foundation through Grant No. CTS-9196004, by the Eastman Kodak Company, and by the Petroleum Research Fund, administered by the American Chemical Society, through Grant ACS-PRF #23284-G7. Computing resources were provided by the San Diego Supercomputer Center.

[1] G. M. Homsy, "Viscous fingering in porous media," Annu. Rev. Fluid Mech. **19**, 271 (1987).
[2] P. G. Saffman and G. I. Taylor, "The penetration of a fluid into a porous medium or Hele–Shaw cell containing a more viscous fluid," Proc. R. Soc. London Ser. A **245**, 312 (1958).
[3] R. L. Chouke, P. van Meurs, and C. van der Poel, "The instability of slow, immiscible, viscous liquid–liquid displacements in permeable media," Trans. AIME **216**, 188 (1959).
[4] C. T. Tan and G. M. Homsy, "Stability of miscible displacements in porous media: Rectilinear flow," Phys. Fluids **29**, 3549 (1986).
[5] Y. C. Yortsos and M. Zeybek, "Dispersion driven instability in miscible displacement in porous media," Phys. Fluids **31**, 3511 (1988).
[6] J.-C. Bacri, N. Rakotomalala, D. Salin, and R. Wouméni, "Miscible viscous fingering: Experiments versus continuum approach," Phys. Fluids A **4**, 1611 (1992).
[7] M. Zeybek and Y. C. Yortsos, "Long waves in parallel flow in Hele–Shaw cells," Phys. Rev. Lett. **67**, 1430 (1991).
[8] M. Zeybek and Y. C. Yortsos, "Parallel flow in Hele–Shaw cells," J. Fluid Mech. **241**, 421 (1992).
[9] E. Meiburg and G. M. Homsy, "Nonlinear unstable viscous fingers in Hele–Shaw flow: II. Numerical simulation," Phys. Fluids **31**, 429 (1988).
[10] E. Brener, H. Levine, and Y. Tu, "Nonsymmetric Saffman–Taylor fingers," Phys. Fluids A **3**, 529 (1991).
[11] C. Canuto, M. Y. Hussaini, A. Quarteroni, and T. A. Zang, *Spectral Methods in Fluid Dynamics*, Springer Series in Computational Physics (Springer-Verlag, New York, 1988).
[12] J. Gary and R. Helgason, "A matrix method for ordinary differential eigenvalue problems," J. Comput. Phys. **5**, 169 (1970).